An experimental and computational study of the vortex shape in a partially baffled agitated vessel

Jean-Philippe Torré[a,b,*], David F. Fletcher[b], Thierry Lasuye[c], Catherine Xuereb[a]

[a] *Laboratoire de Génie Chimique, CNRS UMR 5503, 5 rue Paulin Talabot, BP 1301, 31106 Toulouse, Cedex 01, France*
[b] *Department of Chemical Engineering, The University of Sydney, Australia*
[c] *LVM-Tessenderlo, Mazingarbe, France*

Abstract

The vortex shape in a non-standard partially baffled agitated vessel in the form of a glass-lined, under-baffled stirred vessel has been investigated using both experimental and numerical approaches for an air/water system for different rotation speeds of the agitator. A simple and flexible experimental strategy was developed for determination of the time-averaged location of the unstable free surface using a process involving superimposition of images. CFD simulations were made to predict the vortex shape by using an Eulerian–Eulerian multiphase model coupled with a homogenous turbulence model. The simplifying assumptions of a constant bubble size, a constant drag coefficient and use of the k–ε turbulence model were made. An assessment of the capability of the numerical method to predict the vortex shape was carried out through comparison between experimental data and numerical results. Considering for comparison purposes a water isosurface volume fraction equal to 0.9, to account for the existence of air/water mixture present at the interface in the experiments, instead of the classical value of 0.5, gave very good agreement with the experimental data.

Keywords: Vortex; Partially baffled vessel; Mixing; CFD; Imaging; Interface

1. Introduction

Fluid mixing is carried out in mechanically stirred vessels for a variety of objectives, including for homogenizing single or multiple phases in terms of concentration of components, physical properties and temperature. The choice of the tank geometry, the impeller type and the number and type of baffles can vary depending on the operation carried out.

In the classical geometry, agitated vessels are fitted with baffles which are generally used in the transitional and turbulent flow regimes. Many agitated vessels use standard wall baffles which consist of four flat vertical plates, directed radially, spaced at 90° intervals around the vessel periphery, starting at the bottom tangent line of the lower vessel head and running the length of the vessel side to the top tangent line of the upper head. Most vessels have at least three baffles, with four being the most common, often referred to as a fully baffled condition. When a low viscosity liquid is stirred, the rotating impeller imparts a tangential motion to the liquid and if no baffles are used, the bulk fluid undergoes a swirling motion which approximates solid-body rotation. The fluid moves along circular trajectories with high circumferential velocity creating poor mixing and a vortex is created at the free surface. The fully baffled condition destroys the vortex, keeping the free surface flat, leading to an improved mixing rate and the swirling flow is converted into a preferred flow pattern desirable for process objectives, such as axial flow for blending and solids suspension, or radial flow for dispersions (Myers et al., 2002). For these reasons, baffled tanks are the most widely used in industrial applications and have received much more attention both by experimentalists and modellers (Alcamo et al., 2005; Ciofalo et al., 1996). For further information about baffled tanks, see Brucato et al. (1998) and Harris et al. (1996), who have performed extensive literature reviews of experimental and CFD simulation work on baffled vessels.

Although baffled configurations are encountered in most industrial stirred vessels, there are numerous applications where unbaffled tanks are used. In comparison with baffled vessels, it should be noted that the unbaffled case has been poorly studied in the literature. The vortex, usually regarded as a drawback, may be desirable in a number of situations (see for example Smit and Düring, 1991). The reader can refer to Alcamo et al. (2005), Bakker and Gates (1995), Ciofalo et al. (1996) and Nagata (1975) for considerations on the minimum impeller Reynolds number for which the use of baffles is not required. For further details on the numerous applications where baffles are rarely used (side entering mixers in large product tanks, square or rectangular tanks, etc.), see Paul et al. (2004) and Myers et al. (2002).

In addition to fully baffled, unbaffled and special cases, there exist non-standard baffling applications and in particular partially baffled systems. This category of systems represents stirred baffled tanks that are equipped with baffles but where the baffling effect is not sufficient to prevent vortex formation. These partially baffled vessels are usually encountered in glass-lined vessels. Although a minimum of three baffles are usually used in classical systems to avoid mechanical instability, a one or two baffle configuration is frequent for glass-lined vessels. The type of baffles usually found in glass-lined reactors used for fine chemical and pharmaceutical productions are beaver-tail, H or D type, finger, flattened pipe, fin or concave baffles, as described by Paul et al. (2004). They have no contact with the reactor shell and are usually supported on the vessel heads, rather than being mounted on the vessel wall, in order to prevent chemical fouling and dead zones. To produce good mechanical stability, these baffles hang from flanges attached to the top of the vessel. Due to the limited space available on the head, no more than two baffles are used in glass-lined tanks. Myers et al. (2002) explains that one of the main challenges for baffling in glass-lined vessels arises from the production process. The surface of the baffles must be contoured because sharp corners cannot be coated with glass. As a result, the most common type of baffle used is a pipe flattened to yield an elliptical cross section, commonly called a beaver-tail baffle, and this is the type used in this study. In addition, with only two baffles present, it can be difficult to provide sufficient baffling and glass-lined vessels are usually under baffled.

This study examines the free surface shape in a non-standard partially baffled agitated vessel and the results obtained can be considered as a preliminary analysis of glass-lined under-baffled stirred vessels. The existing experimental methods for the determination of the vortex shape and the numerical method used to simulate it, relative to unbaffled and glass-lined agitated vessels, are briefly reviewed. For unbaffled stirred vessels, construction of a model for the vortex geometry, experimental study of the vortex shape, construction of correlations for the vortex depth and determination of the critical impeller speed at which the gas/liquid interface reaches the impeller, have all received considerable attention from numerous authors for more than 50 years.

Nagata (1975) proposed a simplified theory to describe the vortex geometry. This theory is not detailed in this article but the reader can refer to Ciofalo et al. (1996) who took into account the modified formulation of Smit and Düring (1991). Le Lan and Angelino (1972) measured the vortex shape by electrical contact between a vertical cylindrical electrode of 1 mm diameter and a conducting solution along the entire tank radius. Zlokarnik (1971) observed the vortex through the wall of a transparent vessel and the depth was determined by a plate whose height was infinitely variable and free of parallax. Brennan (1976), who highlighted numerous variables affecting the vortex depth, made graduated marks on the impeller shaft and the vessel wall for measuring the vortex depth and elevation. Photographic analysis was carried out only for stirrer speeds corresponding to stable symmetrical vortices.

Rieger et al. (1979) have also carried out experimental investigations of vortex depth based on visual observations of marks made on the shaft and the vessel wall corresponding to the initial liquid surface position. Ciofalo et al. (1996) have made an assessment of the free surface height by using a vertically adjustable finger movable through the tank diameter. Serra et al. (2001), who investigated turbulent flows in a continuously stirred tank reactor (CSTR) with a free surface, used the interface elevation at the vessel wall to validate the accuracy of the calculations carried out.

Experimental investigations using laser Doppler velocimetry (LDV) and particle image velocimetry (PIV) techniques are extensively reviewed by Mavros (2001), and have also been used to investigate the flow field in unbaffled tanks. In parallel, due to the spectacular progress in digital computing, computational fluid dynamics (CFD) has become a popular and powerful tool and provides detailed analysis of stirred vessels. Armenante and Chou (1994), Armenante et al. (1997) and Dong et al. (1994a,b) experimentally determined the flow field using LDV and numerically predicted it in unbaffled vessels, equipped with a top lid with no head space (i.e., tank completely filled with water inhibiting vortex formation). Lamberto et al. (1999) investigated the laminar flow structure in a stirred tank by PIV and numerical computations, considering the upper surface of the fluid to be flat under conditions where vortex formation did not occur. Murthy Shekhar and Jayanti (2002) carried out flow field simulation of an unbaffled vessel stirred by an eight-blade paddle in laminar, transitional and turbulent flow without a lid and compared the results with the experimental data of Dong et al. (1994a). They considered the top surface as flat with free slip and stated that this may introduce some errors in the formulation of the numerical model, especially at high Reynolds numbers. It was apparent that effects associated with vortex formation and free surface deformation had to be taken into account in the simulation in order to get the correct results. Alcamo et al. (2005) have computed the flow field in an unbaffled stirred tank using large eddy simulation (LES), but again they assumed a flat surface that inhibited vortex formation and any surface aeration.

Glass-lined vessel configurations equipped with a retreat blade impeller have also been investigated by some authors. Campolo and Soldati (2002) and Campolo et al. (2002) made simulations of an industrial size CSTR, equipped with two beaver-tail baffles in a non-symmetrical position, from the

laminar to the fully turbulent regime, for predicting power consumption and pumping efficiency, but they assumed a flat free surface to limit the computational requirements. Li et al. (2004, 2005) carried out LDV measurements and CFD modelling of a stirred vessel equipped with a retreat blade impeller and one cylindrical baffle. The free surface was also treated as a flat, free slip surface.

Very few authors have undertaken the challenge of simulating the flow field including the free surface deformation. In 1996, Ciofalo et al. presented the first simulations of the free surface profile for an unbaffled vessel. The simulations were performed without any empirical data and used a second order turbulence closure model (differential stress model) including the effect of Coriolis forces, implemented in the computer code Harwell-FLOW3D®. An iterative method used with a treatment of non-orthogonal body fitted grids allowed prediction of a vortex shape in good agreement with Nagata's theory (1975) and with vortex height experiments conducted in a model tank. Serra et al. (2001) simulated a baffled CSTR, with coupling between the free surface deformation and a full transient simulation of the flow field. They used a volume of fluid (VOF) method (Jeong and Yang, 1998) with a piecewise linear interface calculation (PLIC) technique (Scardovelli and Zaleski, 1999; Tang et al., 2004) to reconstruct the time evolution of the free surface profile. The time-averaged computed interface trend was captured correctly but some discrepancies between the numerical and experimental results were noted by the authors.

As can be seen from the state-of-the-art described above, the free surface treatment in numerical simulations has often been simplified to allow either comparisons with experimental apparatus equipped with a lid and full of liquid in order to avoid treating numerically the gas/liquid interface or by assuming a flat, stress free surface and neglecting the vortex effects. Concerning the vortex shape which develops in these partially baffled systems, as far as the authors are aware, no experimental or numerical results have been published to date. Thus, two innovative approaches: an experimental one to determine the vortex shape and a numerical one to calculate it using a CFD approach, are presented.

2. Experimental apparatus

The experimental apparatus has been designed to investigate mixing for industrial applications. The pilot-scale equipment comprises a mixing vessel equipped with an agitator system and a camera linked to a computer for video acquisition. The mixing vessel used can be decomposed into distinct elements, which are the bottom dish, the agitation system, the cylindrical part of the vessel placed into a square water filled jacket and the two beaver-tail baffles suspended from the reactor lid. The installation is presented in Fig. 1.

The bottom dish is a curved dish fabricated in steel, drilled in the centre to accommodate a gland packing for rendering the vessel leak tight. The curved shape of the vessel bottom allows the impeller to be placed very close to the bottom, making the reactor suitable for suspending heavy dispersions effectively

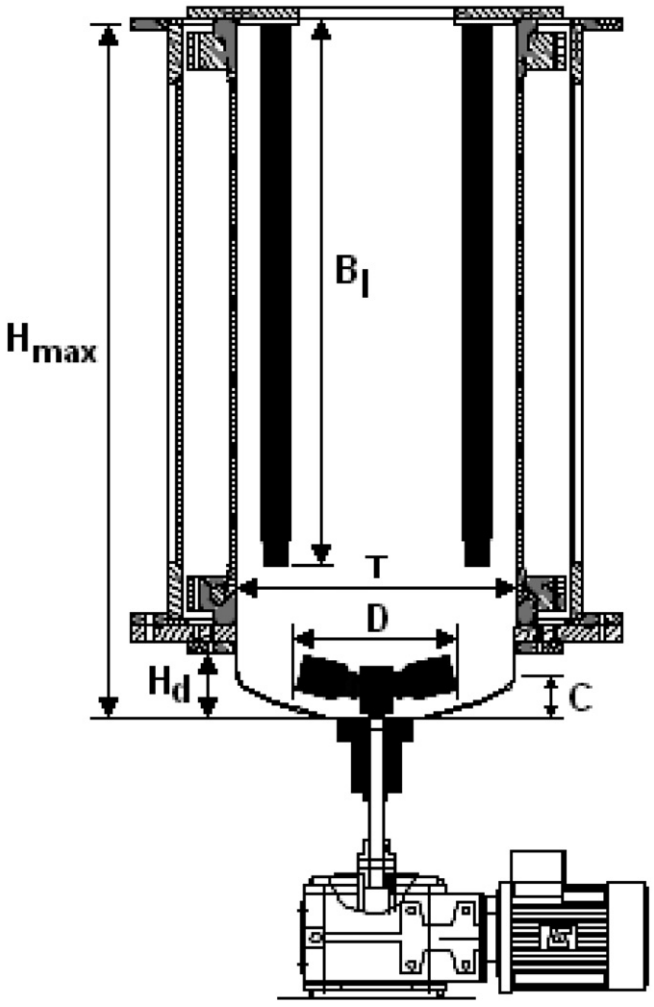

Fig. 1. Schematic of the experimental set-up.

(Li et al., 2005). The cylindrical part of the stirred vessel is composed of a transparent glass column element of 450 mm diameter and 1 m height, allowing a maximum filling volume of 150 l. This part of the vessel is completely contained in a square-section water-filled jacket, made of transparent materials (glass and Perspex Altuglass®) to avoid shell curvature and refraction problems for future laser PIV measurements.

The agitation system is a bottom entering agitator. The three-blade agitator used, shown in Fig. 2, is derived from the standard retreat blade impeller, developed by the Pfaudler Company specifically for glass-lined reactors. This agitator is powered by a 1.5 kW variable speed motor, located below the bottom dish, with a maximum rotation speed of 500 RPM. The two beaver-tail baffles used in the pilot-scale reactor are supported by a flat steel lid fixed on the top of the glass cylindrical vessel part. The dimensions of the baffles and their position inside the vessel are presented in Figs. 1 and 3. Table 1 summarizes all the geometric information for the pilot-scale reactor used in this study.

All the video data acquisition have been made using a commercial Webcam (Philips Toucam Pro II) linked to a standard PC. This Webcam is a commercial camera equipped with a CDD sensor. The information is transferred from the camera to

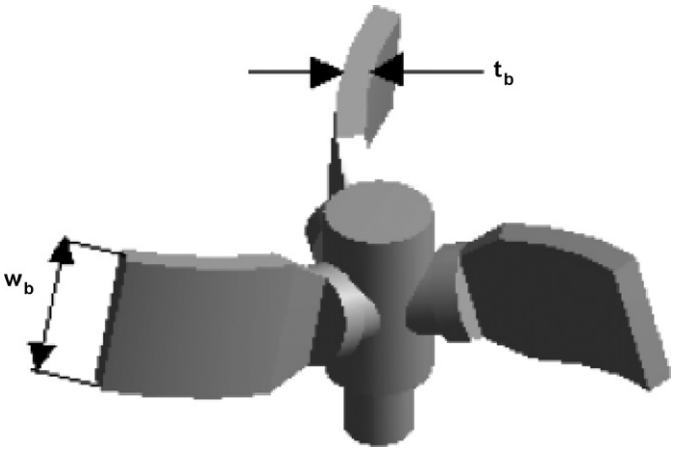

Fig. 2. Geometry of the agitator used in the experiments.

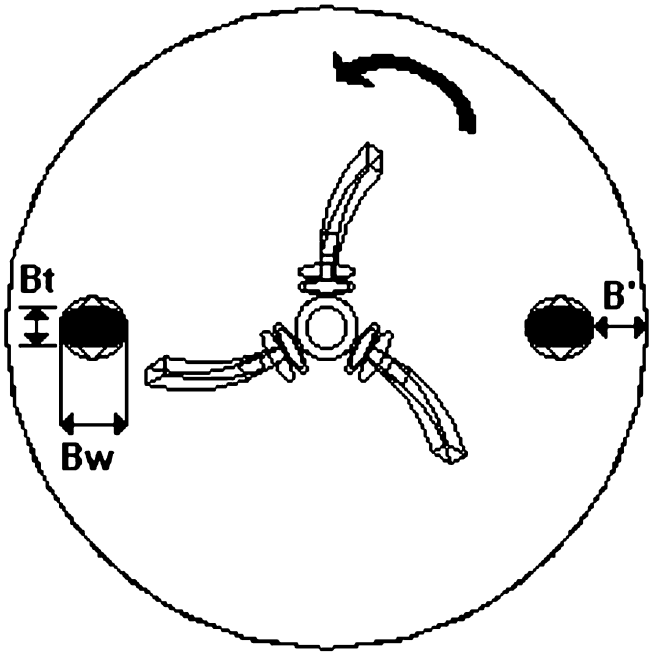

Fig. 3. Plan view of the mixing vessel.

Table 1
Geometric dimensions of the agitated vessel, impeller and baffles

	Symbol	Value
Tank diameter	T	450 mm
Maximum tank height	$H_{\max}$	1156 mm
Bottom dish height	H_{D}	122.9 mm
Agitator diameter	D	260 mm
Number of agitator blades	n_b	3
Agitator blade width	w_b	58 mm
Agitator blade thickness	t_b	9 mm
Agitator retreat angle	θ	15°
Agitator clearance	C	47.2 mm
Baffles length	B_l	900 mm
Number of baffles	n_B	2
Baffle width	B_W	46 mm
Baffle thickness	B_t	27 mm
Distance baffle—reactor shell	B'	38.5 mm

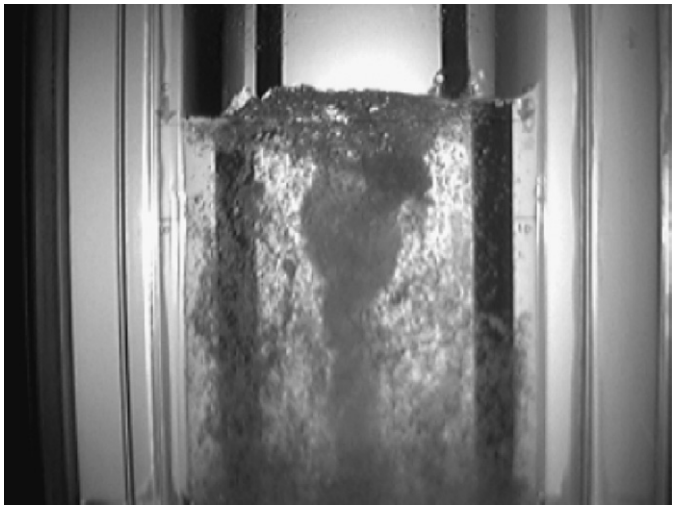

Fig. 4. Picture of the vortex, Webcam ToucamPro II in black and white mode, $N = 275$ RPM, 10 9 1 of water, $H_{\mathrm{init}} = 700$ mm.

the computer via a USB link and the frame rate available can be set from 5 to 60 frames/s. The Webcam was located in front of the tank in order to cover the field necessary to visualise the entire vortex shape. The software used for video post treatment was IRIS 4.17, usually used by amateur astronomers for deep sky or planetary photography. This freeware was downloaded from the internet (http://www.astrosurf.org/buil/iris/iris.htm).

3. Experimental methodology

3.1. Strategy for the experimental acquisition of the vortex shape

One of the main motivations of this study was to develop a simple and effective method for making vortex shape acquisition. The literature study presented earlier highlighted the fact that the experimental methods used by previous authors could only be applied to a stable free surface, as encountered in unbaffled stirred vessels, but could not be used for unstable free surfaces. In contrast, the experimental strategy presented in this study is simple, flexible and requires only readily available equipment.

The stirred tank studied here is a partially baffled system. The two beaver-tail baffles do not have sufficient impact on the solid-body rotation of the fluid to prevent vortex formation, and the vortex free surface is unstable making visualization difficult. Nevertheless, the air/water interface generates a light/dark contrasted area and can be seen qualitatively as a dark shape without well-defined boundaries, as seen in Fig. 4. These fluctuating free surface boundaries can be considered as an unstable phenomenon which has a variable position with time, and the method developed in this study allows easy determination of these boundaries.

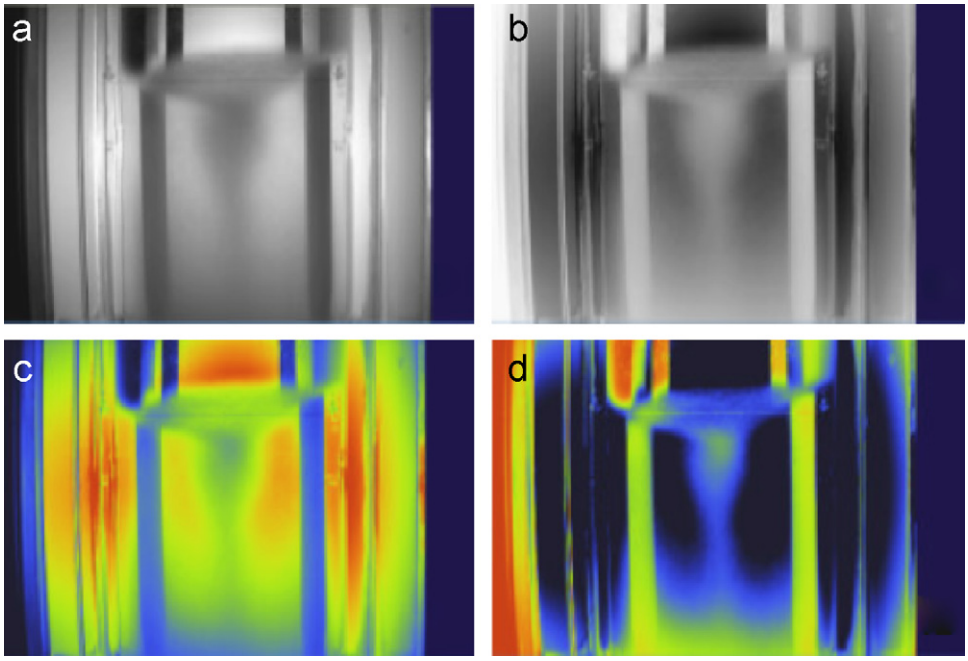

Fig. 5. Final vortex pictures, $N = 275$ RPM. (a) Black and white raw picture; (b) black and white negative picture; (c) coloured picture by transformation of the grey levels of (a) and (d) negative coloured picture from (c) with $G = 21,000$.

The basic idea is that if a phenomenon observed has preferential positions in time, then a video recording with a given frame rate, decomposed into N_F individual frames and the subsequent superimposition of these N_F frames can highlight the most probable area. This idea has been developed with success in this study to highlight a clear vortex shape. The final number of individual frames resulting from the video decomposition is the product of the frame rate and the acquisition time. Classically, the frame rate must be fixed to fit the characteristic time of the physical phenomenon observed. Moreover, the computer buffer limits must be taken into account, as the requirements can become prohibitive if a relative high frame rate from a Webcam is used ($>$ 30 frames/s). The characteristic time of the phenomenon observed does not require a higher frame rate but it can be easily changed for other observations, in smaller tanks for example. Recording during 60 s with a 5 frames/s frame rate was found to be a good compromise between the physics of the system, the acquisition time, the memory allocation and the working computer limits. Thus, all the videos of the following experiments presented in this paper have been recorded with the Webcam during 60 s at a framing rate equal to 5 frames/s.

The camera has been set to black and white mode because the experiments carried out did not require a coloured video acquisition. A black and white acquisition allows treatment of only one channel component during the image post treatment, as opposed to the red, green and blue components, if colour is used. The AVI file generated after acquisition was decomposed into N_F single frames by IRIS and gave 300 frames after decomposition. Then, these N_F frames were superimposed to make the final picture. Several tests with different acquisition times showed that the quality of the final superimposed picture was not improved with a number of frames higher than 300 for the experiments carried out here.

The final picture obtained by the superimposition process is called the raw picture. This raw picture can be easily transformed using IRIS by setting of the image gain, denoted G, with $0 < G < 32,767$, which is used for improving the contrast and increasing the accuracy of free surface mapping. Fig. 5 presents the raw image (a) and three images (b, c and d) obtained by modification of the visualisation parameters following the basic settings available in IRIS from the raw picture. This raw picture was obtained with an initial water level of 700 mm, a rotation speed equal to 275 RPM, an acquisition time of 60 s with a frame rate of 5 frames/s and a superposition of 300 frames to form the final picture. The raw picture (a) can be transformed into a black and white negative (b), a coloured picture proportional to the grey levels of the black and white raw one (c) and finally a negative of the coloured picture presented with the optimal gain equal to 21,000 (d). The case of optimal gain, where a compromise has been made between image quality (low gain) with some loss of information and high gain, where the image quality is poor but all information is retained, gives the best definition of the free surface. We used this basic contrast optimization strategy for all the free surface contour mappings.

3.2. *Calibration procedure*

Using IRIS, it is possible to obtain the pixel coordinates of each point of the picture just by clicking with the mouse on the desired point of the computer screen. Then, an output window allows export of a set of pixel coordinates (X, Y) as a text file which can be used in a spreadsheet program. Due to the change

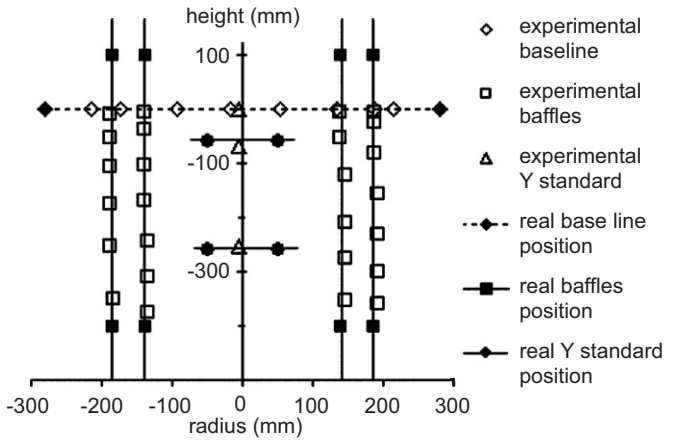

Fig. 6. Comparison between the experimental positions determined from IRIS after calibration (hollow symbols) and real geometrical data of the vessel (full symbols).

of the refraction index between air, water and glass, refraction effects prevent the direct determination of the real geometrical dimensions and these appear larger than they are in reality. So, it was important to calibrate the acquisition method to transform a pixel map given by IRIS into a real geometric map useful for the studies carried out. For the calibration experiments, the stirred vessel was filled with 1091 of water at ambient temperature and the square jacket around the cylindrical part of the reactor was also filled with water at the same temperature to the maximum level. The volume of liquid in the stirred vessel corresponded to the initial water level of 700 mm used in all of the following experiments. A rectangular grid (360 mm × 600 mm) with regular cells (15 mm × 30 mm) was plunged vertically into the reactor in the vortex measurement area, just behind the baffles to determine whether the curvature of the shell led to a non-uniform deformation of lengths in the tank. It was demonstrated that the modification of the grid size was regular on the entire grid and the curvature of the shell has no visible effect. Thus, only one standard for X and one for Y were sufficient for the calibration. The horizontal standard was the distance between the two baffles (281 mm) and the vertical standard was a metallic ruler with two phosphorescent marks spaced 200 mm apart, suspended from the reactor lid into the liquid in a central position. The calibration procedure has been tested for the determination of the real contour and position of the baffles, the initial liquid level and the position of the vertical standard marks.

Fig. 6 represents the comparison between experimental measured points obtained by conversion from the pixel map to the real dimensions with conversion factors for X and Y equal to 5.38 and 4.85, respectively. Good agreement with the reference locations was observed and it was concluded that this method can determine with an uncertainty of ±10 mm the geometrical shapes and positions of locations within the tank.

4. CFD modelling

The numerical simulations were carried out with a commercial CFD package (ANSYS CFX 10.0) to predict the turbulent flow field and the free surface shape in the stirred vessel. The simulation of a free surface implies a separation between gas and liquid caused by the action of body forces and can only be captured by treating the fluid with a multiphase model. The fluids used were water and air at 25 °C in a steady-state simulation. Free surface flows are usually modelled by a VOF model which solves the Navier–Stokes equations, to obtain a common phasic velocity, together with an additional equation that allows determination of the free surface location. In this study, the free surface calculation is made using an Eulerian–Eulerian multiphase model. An inhomogeneous model was chosen to allow phase separation, as a homogeneous model assumes no slip between the liquid and gas, and therefore once fluids mix there is no means to separate them. The interfacial momentum transfer between the two phases was modelled using a disperse phase model in which the liquid phase is continuous and the gas phase is dispersed.

This model is characterized by the solution of an individual set of continuity and momentum set of equations for each phase. The flow field predictions are made via the numerical resolution of the Reynolds-averaged continuity and Navier–Stokes equations. The volume fractions of the phases are tracked with the condition that the volume fractions of all phases sum to unity. The inhomogeneous model applied for the velocity field was coupled with a homogenous turbulence model assuming the turbulent quantities are the same for the two phases, as the phases only co-exist in a small interfacial region. The k–ε turbulence model (Launder and Spalding, 1974) was used in this study for reasons of stability and computational efficiency.

The continuity equation, written for each phase k, is expressed in Eq. (1) by

$$\frac{\partial(\alpha_k \rho_k)}{\partial t} + \nabla \cdot (\alpha_k \rho_k \mathbf{u}_k) = 0, \tag{1}$$

where α_k is the volume fraction, ρ_k is the density and $\mathbf{u}_k$ the phase averaged velocity.

The momentum equation for phase k is written as

$$\begin{aligned}\frac{\partial(\alpha_k \rho_k \mathbf{u}_k)}{\partial t} &+ \nabla \cdot (\alpha_k \rho_k \mathbf{u}_k \otimes \mathbf{u}_k) \\ &= -\alpha_k \nabla P + \nabla \cdot [\mu_k^{\text{eff}} \alpha_k (\nabla \mathbf{u}_k + (\nabla \mathbf{u}_k)^{\text{T}})] \\ &\quad + \alpha_k \rho_k \mathbf{g} + M_{ki},\end{aligned} \tag{2}$$

with

$$\mu_k^{\text{eff}} = \mu_k^{\text{lam}} + \mu_k^{\text{turb}}, \quad \mu_k^{\text{turb}} = \rho_k C_\mu \frac{k^2}{\varepsilon}, \quad C_\mu = 0.09,$$

where $\mathbf{g}$ the acceleration due to gravity and M_{ki} represents the interfacial forces acting on each phase due to the interaction between the two phases. Only drag forces were included for momentum exchange between the two phases. The total drag exerted on the continuous phase by gas per unit volume is given by

$$M_{gl} = \frac{3}{4} \frac{\alpha_g \rho_l}{d_b} C_D |\mathbf{u}_g - \mathbf{u}_l| (\mathbf{u}_g - \mathbf{u}_l), \tag{3}$$

where C_D is the drag coefficient and d_b is an assumed bubble size.

For modelling the vortex shape, two models have been tested for the calculation of the drag coefficient C_D. The first is the modified Schiller–Naumann drag model presented in Eq. (4), and available in CFX 10.0, in which the drag coefficient is modified to ensure the correct limiting behaviour in the inertial regime. Thus, C_D is automatically bounded below with increasing particle Reynolds number (Eq. (6)) and takes a minimum value of 0.44. The second model tested is a constant drag coefficient model (Eq. (5)) usually applied when the particle Reynolds numbers (Eq. (6)) is sufficiently large for inertial effects to dominate over viscous effects.

$$C_D = \mathrm{Max}\left\{\frac{24}{Re_p}(1 + 0.15\,Re_p^{0.687}), 0.44\right\},$$
$$0.1 \leqslant Re_p \leqslant 1\text{–}2 \times 10^5, \tag{4}$$

$$C_D = 0.44, \quad 1000 \leqslant Re_p \leqslant 1\text{–}2 \times 10^5, \tag{5}$$

where

$$Re_p = \frac{\rho_l d_b |u_g - u_l|}{\mu_l}. \tag{6}$$

A multiple reference frame (MRF) model was used in this study. The stirred vessel was separated into regions modelled in rotating frame and stationary frames: the rotating frame is used for the bottom dish containing the rotating impeller, and the stationary frame was used for the cylindrical part of the vessel, containing the cylindrical part of the vessel walls and the two baffles. A no slip condition was set at all solid/liquid interfaces. The boundary condition used on the upper surface of the vessel was the free slip condition, which prevents any flow through the boundary and sets zero gradients for all other quantities. This boundary condition is removed far from the areas of interest and has no significant impact on the results. A frozen rotor condition is set at the interface between the rotating and stationary frames, implying a change of reference frame across the interface but with the relative orientation of the components remaining fixed.

An unstructured grid was used in the simulations. The density of cells was optimized to be fine enough to capture flow details without being excessive. Fig. 7 shows the grid used in the proximity of the right baffle end. Note that inflation meshing was used at all walls. The final mesh, based on sensitivity studies, was composed of 208,000 nodes. All simulations were performed using a second order bounded differencing scheme to limit numerical diffusion as much as possible. The convergence criterion adopted for the simulations is based on the RMS (root mean square) normalized values of the equation residuals. The runs were terminated when the residuals for the mass, momentum and turbulence equations were below 10^{-4}, and below 10^{-3} for the volume fraction equations.

The simulations carried out assumed a liquid height of 700 mm with 100 mm of gas above it. The simulation was initialized with a hydrostatic pressure profile in the liquid phase defined as $P(y) = \rho_l \mathbf{g}(H_l - y)$, for $y \leqslant H_l$.

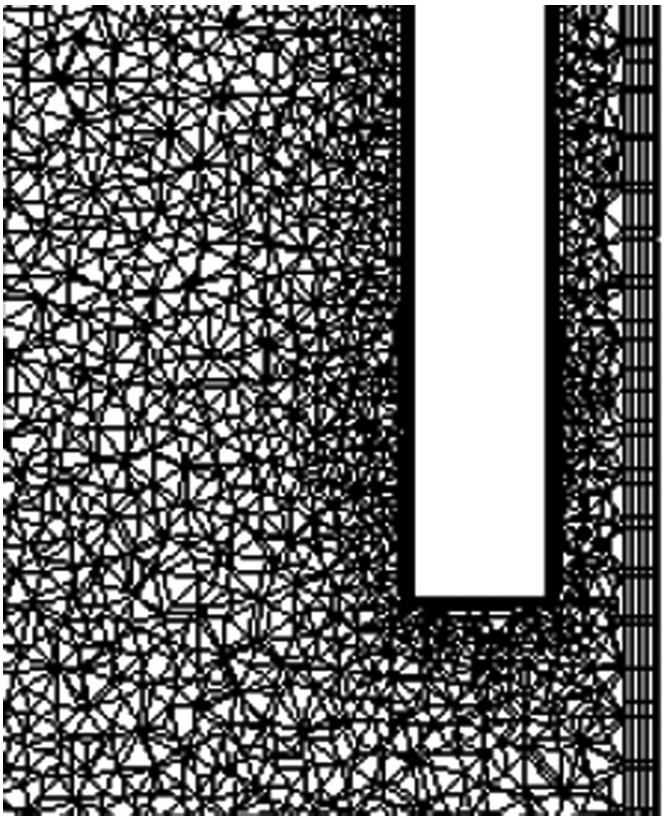

Fig. 7. Unstructured grid used in the simulations in the region near the right baffle bottom tip and the reactor shell.

5. Results and discussion

For unstable free surfaces, as is the case in this study, the process of air bubble formation at the air/water interface, pumping of these down into the liquid due to the liquid velocity field and escape into the gas phase due to the buoyancy force leads to a dynamical system which was hard to treat. The bubble size used for this study was chosen based on physical considerations and results provided by Laakkonen et al. (2005). They used a capillary suction probe technique to measure the local volumetric bubble size distributions in a 0.194 m^3 fully baffled vessel agitated with a Rushton turbine equipped with a ring gas sparger located below the agitator. They found that the Sauter mean diameter measured in the baffle mid-plane close to the surface at 250 RPM for an air-tap water system was close to 3 mm for the two different gas flow rates tested (d_{32} equal to 2.7 and 3 mm, respectively, for air feed rate equal to 0.052 and 0.093 m^3 (gas) m^{-3} (dispersion) min^{-1}). Whilst this situation is different to ours, it provides a guide to the likely stable bubble size in this system. Our results were found to be insensitive to moderate changes to the bubble diameter (bubble sizes in the range 1–3 mm were tested) with a 3 mm size giving the best convergence. Thus, a constant bubble diameter of 3 mm was adopted for the following simulations.

Concerning the drag coefficient model, the comparison between numerical prediction of the vortex shapes at 275 RPM using a modified Schiller–Naumann drag coefficient model or

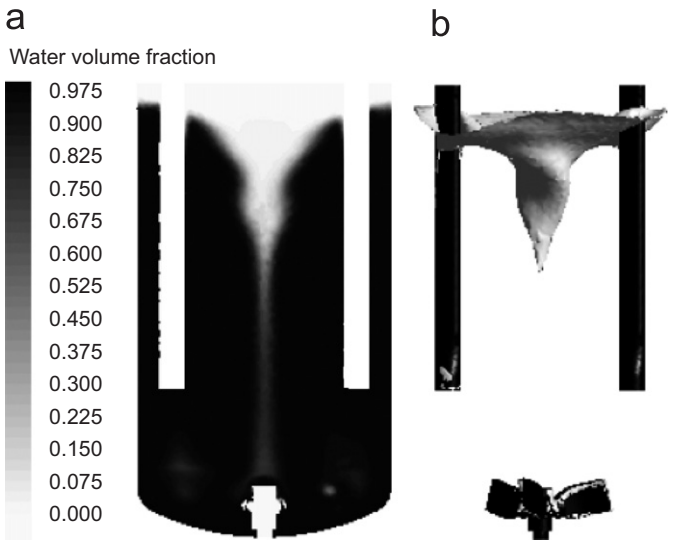

Fig. 8. (a) Water volume fraction profile with $N = 275$ RPM and (b) isosurface of water volume fraction equal to 0.5.

a constant drag coefficient equal to 0.44 led to identical vortex shapes. Thus, the simplest model (Eq. (5)), was adopted for the remainder of the computational calculations. In this system there is obviously a complex interaction between the phases as bubbles of various sizes mix at the interface and disentrain due to buoyancy. The bubble size and drag coefficient were chosen to give a physically realistic estimate of the drag force between the gas and liquid. Here we are not trying to model this process in detail but rather we assume a fixed bubble size and a constant drag coefficient that provide sufficient slip at the interface to represent this process.

The vortex surface, being physically the interface between the gas and the liquid, was obtained from the simulations by the 3D representation of a water isosurface volume fraction. Fig. 8a and b show the water volume fraction profile obtained at 275 RPM and the corresponding vortex represented by a water volume fraction isosurface of 0.5, respectively. To compare the planar image view with the experimental results, a projection of the free surface onto the vertical XY baffle plane has been made, considering only the X and Y coordinates of the vortex shape (the Z coordinate being normal to the baffle plane).

Firstly, the influence of the value of the water volume fraction used to determine the free surface shape has been investigated for a constant rotation speed of 275 RPM from 0.5 to 0.95. Fig. 9 compares the experimental vortex shape determined at the optimal gain (21,000) with an isosurface of water volume fraction equal to 0.5 (Fig. 9a) and 0.9 (Fig. 9b). These comparisons lead to several comments. The experimental results and the numerical prediction give the same global vortex shape. It can be noted that the numerical predictions of the curvatures of the vortex boundary in its central part (the bulb shape) and the maximum liquid height (median or lateral parts) are in relatively good agreement with the experimental results.

In addition, the water volume fraction used for the calculation of the isosurface representing the vortex has a significant

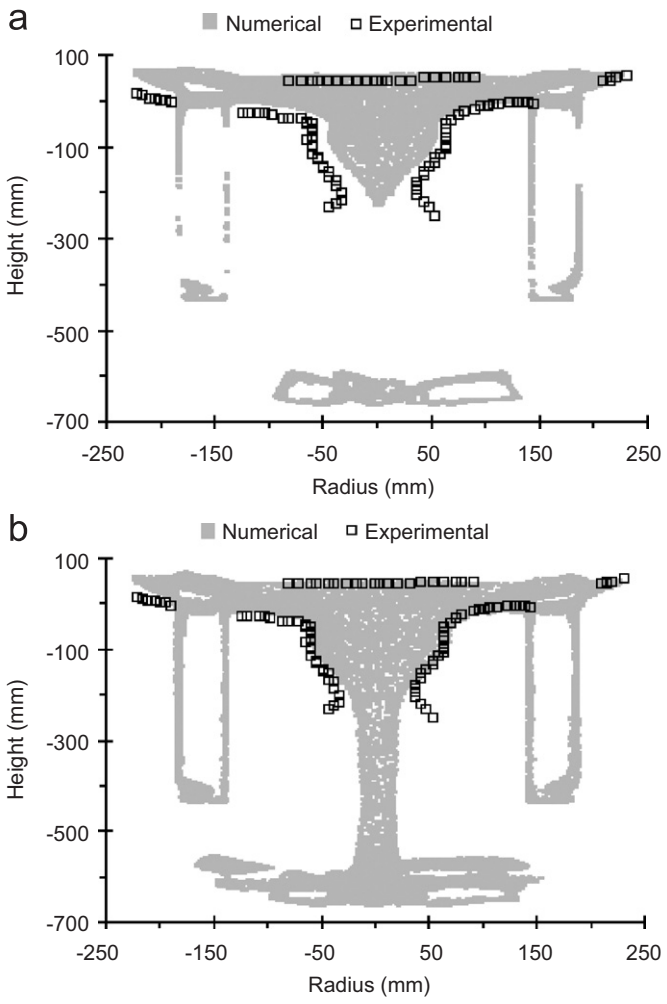

Fig. 9. Comparison between experimental vortex shape profile (negative coloured picture, $G = 21,000$, $N = 275$ RPM) and the projection on the XY vertical plane of isosurfaces of water volume fraction ($N = 275$ RPM); (a) isosurface of water volume fraction equal to 0.5 and (b) isosurface of water volume fraction equal to 0.9.

influence on the comparison. The small gradient of water volume fraction profile around the gas/liquid interface is sufficient to give a difference in the free surface representation. It may be seen that the use of a water volume fraction of 0.9 instead of 0.5 leads to better agreement between the experimental results and the numerical predictions. This may be due to the experimental strategy for vortex shape capture. The image picture method is very sensitive to a small percentage of gas mixed into the liquid phase. It is clearly visible that the imaging process does not differentiate between the high volume fraction of gas present in the vortex core and the bubbles pumped down by the agitation effect into the liquid at the bottom tank. The free surface boundary, which represents the vortex shape, is a region of dynamical equilibrium, where gas bubbles are introduced into the liquid and subsequently come out again into the vortex core. Thus, this dynamical area of intense gas movement could be captured by the camera and included in the free surface shape. This may explain why the experimental data are

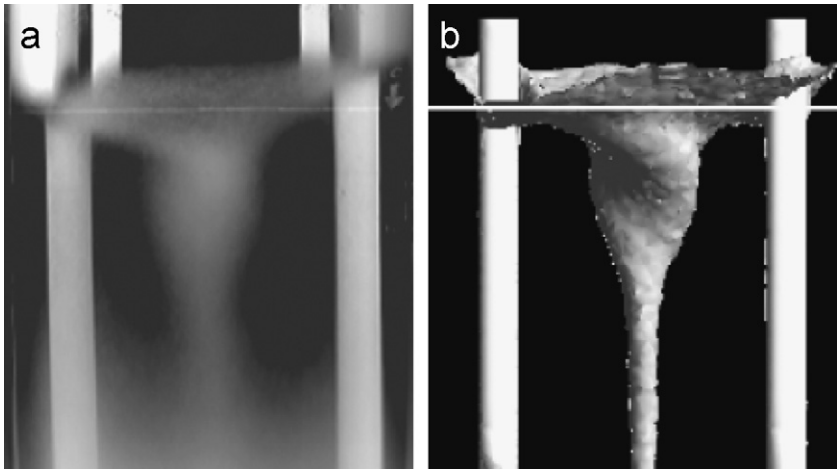

Fig. 10. Comparison on the same scale of the experimental (a) and the numerical (b) vortex shapes; (a) negative coloured picture, $G = 21,000$, $N = 275$ RPM and (b) isosurface of water volume fraction equal to 0.9 ($N = 275$ RPM).

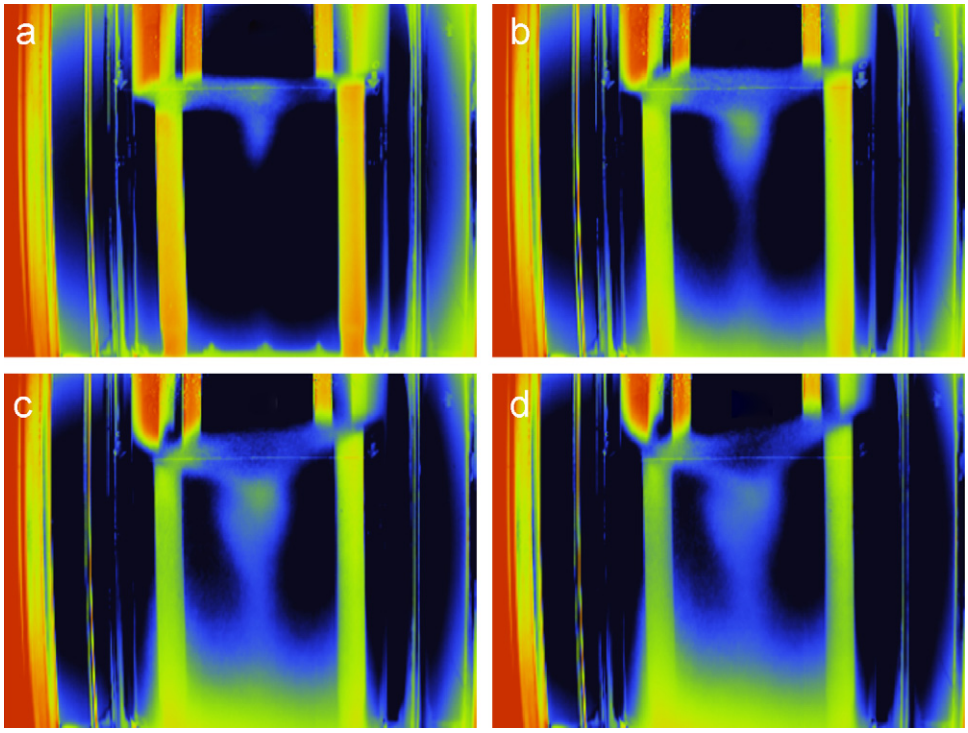

Fig. 11. Experimental acquisitions of the vortex shapes, negative coloured pictures: (a) $N = 200$ RPM, $G = 26,000$; (b) $N = 250$ RPM, $G = 22,500$; (c) $N = 300$ RPM, $G = 20,000$; (d) $N = 350$ RPM, $G = 18,000$.

closer to the numerical predictions made with a water volume fraction equal to 0.9. Alternatively, the numerical model and particularly the use of an interfacial term M_{ki} including only the drag force could play an important role in the prediction of the water volume fraction profile. The interfacial forces acting on the gas bubbles should also contain the Basset, virtual mass and lift forces, but these have been neglected in the present simulations. If they are included, one may arrive at a different value for the water volume fraction that best fits the experimental profiles in Figs. 9 and 12. Fig. 10 shows the comparison between the experimental image of the vortex shape for 275 RPM and the numerical isosurface of water volume fraction equal to 0.9 represented at the same scale. Very good agreement is shown between these two figures.

Further results have been obtained for additional impeller speeds (200, 250, 300 and 350 RPM). Figs. 11 and 12 contain the results. Good agreement between the experimental data and numerical predictions was observed with the global vortex shape at 250 and 300 RPM. The maximum height reached by the liquid, the bottom vortex contour located between the baffles

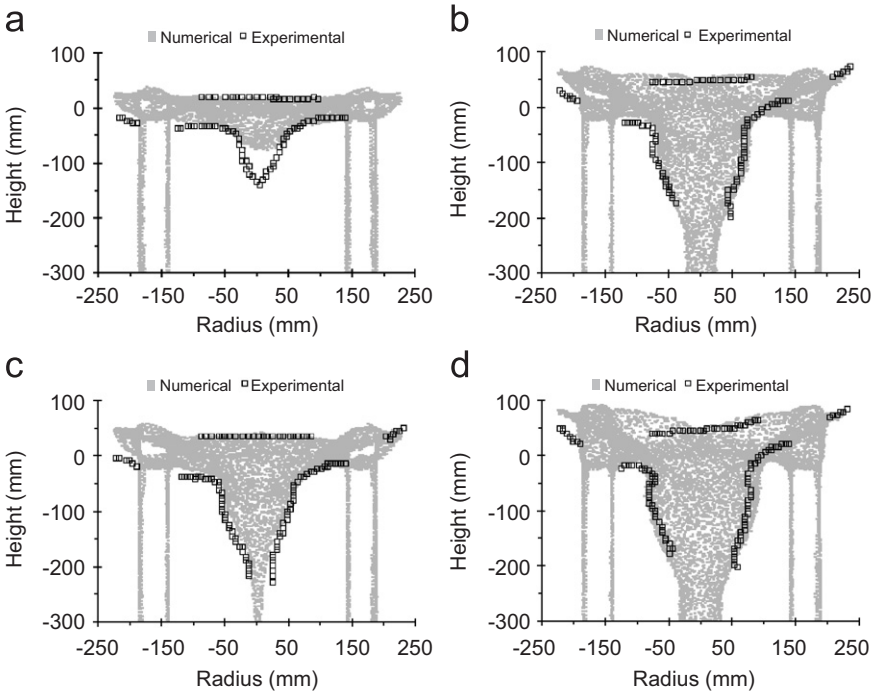

Fig. 12. Comparison between experimental vortex shapes (negative coloured pictures with the optimal gain) and the projection on the XY vertical plane of isosurfaces of water volume fraction equal to 0.9: (a) 200 RPM; (b) 250 RPM; (c) 300 RPM and (d) 350 RPM.

and the central vortex bulb and the periphery of the bulb shape vortex were predicted in satisfactory agreement with the experimental results. At 200 RPM, both the numerical and experimental vortex profiles showed a "closed" vortex, in the sense that the vortex bottom could be located precisely, contrary to the vortex shapes observed at higher rotation speeds. Nevertheless, some discrepancies were noted at the lowest (200 RPM) and the highest (350 RPM) impeller rotation speeds tested. At 200 RPM, the experimental vortex was deeper than the numerical results. It is hypothesized that the small central core was not captured in the experimental work, as the recorded flat base is not consistent with the expected shape. At 350 RPM, the experimental acquisition was uncertain due to the very high number of bubbles pumped down into the tank and rotating into the bulk. In addition, the thickness of the air/water zone around the free surface was wider, increasing the measurement uncertainties of the vortex contour.

6. Conclusions

The vortex shape that develops in a non-standard, partially baffled, agitated vessel of 450 mm diameter, similar to glass-lined under-baffled stirred vessels, has been studied both experimentally and numerically. The strong instability of the free surface due to the dynamic process of bubble formation and pumping at the air/water interface accompanied by gas disengagement lead to the development of a novel experimental strategy to measure the vortex shape. A video acquisition method based on the superposition of images was used and showed the capability to determine accurately the position of the vortex contours at different rotation speed from 200 to 350 RPM.

The vortex shape was also predicted numerically by CFD using an Eulerian–Eulerian multiphase approach, coupled with post-processing in the form of volume fraction isosurface profiles. An assessment of the capability of the numerical method to predict the vortex shape was carried out through comparison between experimental data and numerical results. Even with the use of a homogeneous k–ε turbulence model and the approximations of a single bubble diameter and a constant drag used in the CFD calculations, the numerical model was able to give a vortex shape in very good agreement with the experimental data from 250 to 350 RPM. Instead of the classical value of a water isosurface volume fraction equal to 0.5, the value of 0.9 gives the best agreement with experimental data due to the presence of the dynamical equilibrium zone of intense gas/liquid exchanges which occurs around the free surface into the air zone. Although the modelling of the detailed gas entrainment and disentrainment process was not carried out in this study, it is a challenging problem to take into account in future work.

Notation

B'	distance baffle-reactor shell, mm
B_l	baffles length, mm
B_t	baffle thickness, mm
B_w	baffle width, mm
C	agitator clearance, mm
C_μ	k–ε model constant, dimensionless
C_D	drag coefficient, dimensionless

d_{32}	Sauter mean bubble diameter, mm
d_b	bubble diameter, mm
D	agitator diameter, mm
$\mathbf{g}$	gravity acceleration, $m^2\,s^{-1}$
G	gain value of the IRIS image treatment software, dimensionless
H_D	bottom dish height, mm
H_{init}	initial water level for the experiments carried out, mm
H_l	liquid height, mm
$H_{\max}$	maximum tank height, mm
k	turbulent kinetic energy, $m^2\,s^{-2}$
M_{gl}	drag force per unit volume, $N\,m^{-3}$
M_{ki}	interfacial forces per unit volume, $N\,m^{-3}$
n_B	number of agitator blades, dimensionless
N	agitator rotation speed, RPM
N_b	number of baffles, dimensionless
N_F	number of frames superimposed during the imaging process, dimensionless
P	pressure, Pa
Re	Reynolds number, dimensionless, $Re = \rho_l N D^2/\mu_l$
Re_p	Particle Reynolds number, dimensionless, $Re_p = \rho_l d_b \lvert u_g - u_l \rvert/\mu_l$
t_b	agitator blade thickness, mm
t	time, s
T	tank diameter, mm
$\mathbf{u}$	velocity, $m\,s^{-1}$
$\mathbf{u}'$	velocity fluctuation, $m\,s^{-1}$
w_b	agitator blade width, mm

Greek letters

α	volume fraction, dimensionless
ε	dissipation rate of turbulent energy per unit volume, $m^2\,s^{-3}$
θ	agitator retreat angle, degrees
μ	dynamic viscosity, $kg\,m^{-1}\,s^{-1}$
ρ	density, $kg\,m^{-3}$

Subscripts

g	gas phase
i	interfacial
k	phase index
l	liquid phase

Superscripts

eff	effective
lam	laminar
T	matrix transposition
turb	turbulent

Acknowledgements

The authors would like to express their gratitude to Tessenderlo Group and the ANRT for the financial support of this work (CIFRE/ANRT contract No. 1727/1413582.00). They also would like to thank Dr. Dirk Van Deynse, Tessenderlo Chemie Group Research and Development Director, Mr. Marc Branly, Technical Department Manager of the LVM plant of Mazingarbe (F), Wiel Felder, Technical Department Manager of the LVM plant of Beek (NL) and Maurice Steffin, Process Engineer of the LVM plant of Beek (NL) for their valuable contribution and advice. We would also like to thank Alain Muller, Lahcen Farhi, Jacques Labadie, Marc Samazan, Eric Panader and Gilles Millet, technical personnel of the Chemical Engineering Laboratory of Toulouse, for their work on the pilot reactor design and assembly.

References

Alcamo, R., Micale, G., Grisafi, F., Brucato, A., Ciofalo, M., 2005. Large-eddy simulation of turbulent flow in an unbaffled stirred tank driven by a Rushton turbine. Chemical Engineering Science 60 (8–9), 2303–2316.

Armenante, P.M., Chou, C.-C., 1994. Experimental LDV measurement and numerical CFD determination of the fluid velocity distribution in an unbaffled mixing vessel. AIChE Symposium Series 90 (299), 33–40.

Armenante, P.M., Luo, C., Chou, C.-C., Fort, I., Medek, J., 1997. Velocity profiles in a closed, unbaffled vessel: comparison between experimental LDV data and numerical CFD predictions. Chemical Engineering Science 52 (20), 3483–3492.

Bakker, A., Gates, L.E., 1995. Properly choose mechanical agitators for viscous liquids. Chemical Engineering Progress 91 (12), 25–34.

Brennan, D.J., 1976. Vortex geometry in unbaffled vessels with impeller agitation. Transactions of the Institution of Chemical Engineers 54, 209–217.

Brucato, A., Ciofalo, M., Grisafi, F., Micale, G., 1998. Numerical prediction of flow fields in baffled stirred vessels: a comparison of alternative modelling approaches. Chemical Engineering Science 53 (21), 3653–3684.

Campolo, M., Soldati, A., 2002. Appraisal of fluid dynamic efficiency of retreated blade and turbofoil impellers in industrial-sizes CSTRs. Industrial & Engineering Chemistry Research 41, 1370–1377.

Campolo, M., Paglianti, A., Soldati, A., 2002. Fluid dynamic efficiency and scale-up of a retreated blade impeller CSTR. Industrial & Engineering Chemistry Research 41, 164–172.

Ciofalo, M., Brucato, A., Grisafi, F., Torraca, N., 1996. Turbulent flow in closed and free-surface unbaffled tanks stirred by radial impellers. Chemical Engineering Science 51 (14), 3557–3573.

Dong, L., Johansen, S.T., Engh, T.A., 1994a. Flow induced by an impeller in an unbaffled tank (I): experimental. Chemical Engineering Science 49 (4), 549–560.

Dong, L., Johansen, S.T., Engh, T.A., 1994b. Flow induced by an impeller in an unbaffled tank (II): numerical modelling. Chemical Engineering Science 49 (20), 3511–3518.

Harris, C.K., Roekaerts, D., Rosendal, F.J.J., Buitendijk, F.G.J., Daskopoulos, Ph., Vreenegoor, A.J.N., Wang, H., 1996. Computational fluid dynamics for chemical reactor engineering. Chemical Engineering Science 51 (10), 1569–1594.

Jeong, J.H., Yang, D.Y., 1998. Finite element analysis of transient fluid flow with free surface using the VOF (Volume-Of-Fluid) method and adaptative grid. International Journal for Numerical Methods in Fluids 26, 1127–1154.

Laakkonen, M., Moilanen, P., Aittamaa, J., 2005. Local bubble size distributions in agitated vessels. Chemical Engineering Journal 106 (2), 133–143.

Lamberto, D.J., Alvarez, M.M., Muzzio, F.J., 1999. Experimental and computational investigation of the laminar flow structure in a stirred tank. Chemical Engineering Science 54 (7), 919–942.

Launder, B.E., Spalding, D.B., 1974. The numerical computation of turbulent flows. Computer Methods in Applied Mechanics and Engineering 3, 269–289.

Le Lan, A., Angelino, H., 1972. Etude du vortex dans les cuves agitées. Chemical Engineering Science 27 (11), 1969–1978.

Li, M., White, G., Wilkinson, D., Roberts, K.J., 2004. LDA measurements and CFD modelling of a stirred vessel with a retreat curve impeller. Industrial & Engineering Chemistry Research 43, 6534–6547.

Li, M., White, G., Wilkinson, D., Roberts, K.J., 2005. Scale up study of retreat curve impeller stirred tanks using LDA measurements and CFD simulation. Chemical Engineering Journal 108 (1–2), 81–90.

Mavros, P., 2001. Flow visualization in stirred vessels, a review of experimental techniques. Transactions of the Institution of Chemical Engineers 79 (A), 113–127.

Murthy Shekhar, S., Jayanti, S., 2002. CFD study of power and mixing time for paddle mixing in unbaffled vessels. Transactions of the Institution of Chemical Engineers 80 (A), 482–498.

Myers, K.J., Reeder, M.F., Fasano, J.B., 2002. Optimize mixing by using the proper baffles. Chemical Engineering Progress 91 (12), 25–34.

Nagata, S., 1975. Mixing: Principles and Applications. Wiley, New York.

Paul, E.L., Atiemo-Obeng, V.A., Kresta, S.M., 2004. Handbook of Industrial Mixing: Science and Practise. Wiley, Hoboken, NJ.

Rieger, F., Ditl, P., Novák, V., 1979. Vortex depth in mixed unbaffled vessels. Chemical Engineering Science 34 (3), 397–403.

Scardovelli, R., Zaleski, S., 1999. Direct numerical simulation of free-surface and interfacial flow. Annual Review of Fluid Mechanics 31, 567–603.

Serra, A., Campolo, M., Soldati, A., 2001. Time-dependent finite-volume simulation of the turbulent flow in a free-surface CSTR. Chemical Engineering Science 56 (8), 2715–2720.

Smit, L., Düring, J., 1991. Vortex geometry in stirred vessel. Proceedings of the Seventh European Congress on Mixing, Part II, Brugge, Belgium, pp. 633–639.

Tang, H., Wrobel, L.C., Fan, Z., 2004. Tracking of immiscible interfaces in multiple-material mixing processes. Computational Materials Science 29 (1), 103–118.

Zlokarnik, M., 1971. Trombentiefe beim rühren in unbewehrten behältern. Chemie Ingenieur Technnik 43 (18), 1028–1030.